JNeurosci
THE JOURNAL OF NEUROSCIENCE

Research Articles: Cellular/Molecular

Glial-Specific Deletion of Med12 Results in Rapid Hearing Loss via Degradation of the Stria Vascularis

https://doi.org/10.1523/JNEUROSCI.0070-21.2021

Cite as: J. Neurosci 2021; 10.1523/JNEUROSCI.0070-21.2021

Received: 12 January 2021
Revised: 11 June 2021
Accepted: 5 July 2021

Glial-Specific Deletion of Med12 Results in Rapid Hearing Loss via Degradation of the Stria Vascularis

Teng-Wei Huang[1], Amrita A. Iyer[3,6], Jeanne M. Manalo[4], Junsung Woo[1], Navish A. Bosquez Huerta[1,5], Melissa M. McGovern[2], Heinrich Schrewe[7], Fredrick A. Pereira[8,9], Andrew K. Groves [2,3,5,6], Kevin K. Ohlemiller [10], and Benjamin Deneen [1,2,5,11] *

[1] Center for Cell and Gene Therapy, Baylor College of Medicine, Houston TX 77030

[2] Department of Neuroscience, Baylor College of Medicine, Houston TX 77030

[3] Department of Molecular and Human Genetics, Baylor College of Medicine, Houston TX 77030

[4] Department of Biochemistry and Molecular Biology, The University of Texas Health Science Center at Houston, Houston TX

[5] Program in Developmental Biology, Baylor College of Medicine, Houston TX 77030

[6] Program in Genetics & Genomics, Baylor College of Medicine, Houston TX 77030

[7] Department of Developmental Genetics, Max Planck Institute for Molecular Genetics, Berlin Germany

[8] Huffington Center on Aging, Baylor College of Medicine, Houston TX 77030

[9] Department of Otolaryngology, Baylor College of Medicine, Houston TX 77030

[10] Department of Otolaryngolgy, Central Institute for the Deaf, Fay and Carl Simons Ctr. for Biology of Hearing and Deafness , Washington University, St. Louis MO 63110

[11] Department of Neurosurgery, Baylor College of Medicine, Houston TX 77030

* Correspondence: Benjamin Deneen, deneen@bcm.edu

Abbreviated Title: Glial Expression of Med12 Regulates Adult Hearing

Number of Pages: 34

Number of Figures: 7 Figures

Abstract Words: 159

Introduction Words: 598

Discussion Words: 900

Conflict of Interest Statement: Authors declare no conflicts of interest

Acknowledgements: This work was supported by grants from the National Multiple Sclerosis Society (FG-1607-25417, to TH) and the NIH (NS071153 and NS096096, to BD and DC014832 to AG). AAI was supported in part by The Cullen Foundation.

Abstract

Mediator protein complex subunit 12 (Med12) is a core component of the basal transcriptional apparatus and plays a critical role in the development of many tissues. Mutations in Med12 are associated with X-linked intellectual disability syndromes and hearing loss; however, its role in nervous system function remains undefined. Here, we show that temporal conditional deletion of Med12 in astrocytes in the adult central nervous system results in region specific alterations in astrocyte morphology. Surprisingly, behavioral studies revealed rapid hearing loss after adult deletion of Med12 that was confirmed by a complete abrogation of auditory brainstem responses. Cellular analysis of the cochlea revealed degeneration of the stria vascularis, in conjunction with disorganization of basal cells adjacent to the spiral ligament and downregulation of key cell adhesion proteins. Physiological analysis revealed early changes in endocochlear potential, consistent with strial-specific defects. Together, our studies reveal that Med12 regulates auditory function in the adult by preserving the structural integrity of the stria vascularis.

Significance Statement

Mutations in Mediator protein complex subunit 12 (Med12) are associated with X-linked intellectual disability syndromes and hearing loss. Using temporal-conditional genetic approaches in CNS glia, we found that loss of Med12 results in severe hearing loss in adult animals through rapid degeneration of the stria vascularis. Our study describes the first animal model that recapitulates hearing loss identified in Med12-related disorders and provides a new system in which to examine the underlying cellular and molecular mechanisms of Med12 function in the adult nervous system.

Introduction

Glial cell support of neuronal function is a hallmark feature of nervous systems across evolution, with both glial abundance and specialization correlated with increasing neuronal- and organism-complexity (Freeman & Rowitch 2013). Accordingly, mammalian systems contain a host of specialized glial cells that subserve neuronal function, with astrocytes serving as an archetype for glial support (Allen & Lyons 2018, Nagai et al 2020). Among the key functions performed by astrocytes include buffering neurotransmitters, maintenance of ion gradients, and providing metabolic support, all of which directly influence the function of neurons and associated circuits (Khakh & Deneen 2019).

In the mammalian auditory system hair cells use mechanosensation to convert energy from soundwaves into neurophysiological signals that are transmitted to the brainstem (Brownell et al 1985, Chan & Hudspeth 2005, Muller 2008) Hair cell function relies on the endocochlear potential, which is an ion gradient established in the endolymph and maintained by the stria vascularis (Gulley & Reese 1976, Patuzzi 2011). The resting potential of the endolymph is regulated by the transport of K^+ ions across the stria vascularis into the cochlear duct (Boettger et al 2002, Grunder et al 2001, Mittal et al 2017). This function is mediated by potassium channels, including Kir4.1 which is the predominant channel used by astrocytes to buffer neuronal K^+ (Chen & Zhao 2014, Rozengurt et al 2003). Critically, disruption of these electrochemical gradients in the endolymph can lead to altered hair cell function and survival, culminating in a loss of hearing (Mittal et al 2017, Nin et al 2016). While much progress has been made in

92 understanding how the stria vascularis regulates endocochlear potential, the
93 transcriptional mechanisms that control stria vascularis function remain poorly defined.
94 Glial development offers a venue in which to identify transcription factors that
95 regulate mature glial cell function. For example, Sox10 and NFIA are key regulators of
96 oligodendrocyte and astrocyte development, respectively, and the physiological
97 functions of these cells in the adult CNS (Huang et al 2020, Stolt et al 2002). These
98 parallels also apply to auditory support cells, where Sox2, Sox9, and Sox10 are
99 expressed in developing and mature CNS glia and support cells in the cochlea
100 (Loponen et al 2011, Oesterle et al 2008, Watanabe et al 2000). Drawing on this parallel,
101 we identified Mediator Complex Subunit 12 (Med12) as a developmental transcription
102 factor that is enriched in subsets of astrocytes in the adult brain (John Lin et al 2017).
103 Studies in development have shown that Med12 cooperates with Sox10 to regulate
104 oligodendrocyte differentiation (Vogl et al 2013), however its role in mature astrocytes is
105 undefined. Furthermore, mutations in Med12 are linked to intellectual disability
106 syndromes and coupled with hearing loss (Donnio et al 2017, Lesca et al 2013,
107 Rubinato et al 2020, Schwartz et al 2007, Vulto-van Silfhout et al 2013). These
108 observations implicate Med12 as a critical transcription factor contributing to a host of
109 nervous systems functions related to neuronal circuits, myelination, and auditory
110 function. Despite its widespread expression in neurons and glia, the precise role of
111 Med12 in the adult CNS remains unknown.
112 To dissect the contributions of Med12 towards brain function we generated
113 temporal-conditional mouse knockout models that enabled us to delete Med12 in
114 astrocytes. Analysis across brain regions revealed reduced astrocyte complexity in the

hippocampus, while behavioral studies revealed that mice lacking astrocytic-Med12 are deaf and have no auditory brainstem response. Cellular analysis of the cochlea revealed that Med12 is required to maintain the integrity of the stria vascularis, which eventually results eventual loss of hair cells. Together, these studies identify Med12 in the stria vascularis as a key regulator of auditory function.

Materials and Methods

Animals

All experimental animals were treated in compliance with the US Department of Health and Human Services, the NIH guidelines, and Baylor College of Medicine IACUC guidelines. All mice were housed with food and water available ad libitum in a 12-hour light/dark environment. Both female and male mice were used for all experiments, and littermates of the same sex were randomly allocated to experimental groups. For histological analyses of brains and behavior assays, adult mice aged 4-month were used unless otherwise described. For auditory brainstem response (ABR) test and histological analyses of inner ears, examinations or tissue collections were performed at either 1, 2, 3, or 5 weeks after the tamoxifen treatment as described. All mice used in this study were maintained on the C57BL/6J background. Med12 conditional knockout mice were generated by crossing Med12 fl/fl or fl/y conditional mutant mice (Rocha et al., 2010) with Aldh1l1-CreER (The Jackson Laboratory; RRID:IMSR_JAX:029655), resulting in Med12fl/fl; Aldh1l1-CreER or Med12fl/y; Aldh1l1-CreER (A12-KO) and Med12fl/fl or Med12fl/y (A12-Con) littermate controls. For histological analysis, the

Aldh1l1-GFP mouse was crossed with A12-KO, resulting in Med12fl/fl (or Med12fl/y); Aldh1l1-CreER; Aldh1l1-GFP (AG12-KO) and Med12fl/fl (or Med12fl/y); Aldh1l1-GFP (AG12-Con) mice. To mark the Cre-targeted cells, Rosa-CAG-LSL-tdTomato-WPRE mice was crossed with A12-KO, resulting in Med12fl/fl (or Med12fl/y); Aldh1l1-CreER; Rosa-CAG-LSL-tdTomato-WPRE (AT12-KO) and Med12+/+ (or Med12+/y); Aldh1l1-CreER; Rosa-CAG-LSL-tdTomato-WPRE (AT12-Con) mice. To induce deletion of Med12 in the adult, four-week-old mice were gavage-fed with 150 mg/kg body weight of Tamoxifen (Sigma-Aldrich, cat no. T5648) dissolved in corn oil twice per day for 5 days. Above experiments were approved by Baylor College of Medicine IACUC.

Immunofluorescence on frozen tissue sections

Mice were anesthetized under isoflurane inhalation and perfused transcardially with 1X PBS pH 7.4 followed by 4% paraformaldehyde (PFA). Brains were removed, post-fixed in 4% PFA for 8 hours, and placed in 20% sucrose for 16 hours before embedded in OCT. Inner ears were dissected from temporal bones and fixed in 4% PFA overnight, decalcified in 0.2 M EDTA for 24 hours. Decalcified inner ears were incubated in 7.5% gelatin solution (1X PB/10% sucrose) at 37°C for 1 hour before embedded in OCT. Brain sections of 30 μm and cochlea sections of 12 μm were made on a cryostat. For immunostaining, tissue sections were washed with 1X PBS 5 min X3, blocked with 10% goat serum in PBS with 0.3% Tween20, and then incubated with primary antibodies in blocking solution overnight. On the next day, sections were incubated with secondary antibodies in PBS with 0.1% Tween20 for 1 h RT, followed by incubation with DAPI for 5 min, and mounted with VECTASHIELD Antifade Mounting Media (Vector Laboratories,

H-1000). The following primary antibodies were used: Chicken anti-GFP (1:1000; abcam, ab13970), rabbit anti-Med12 (1:1000; Novus Biologicals, NB100-2357), chicken anti-GFAP (1:1000; abcam, ab4674), mouse anti-GFAP (1:1000, EMD millipore, MAB360), mouse anti-NeuN (1:500, millipore, MAB377), rabbit anti-Myosin-VIIa (1:1000, Proteus BioSciences, 25-6790), mouse anti-Myosin-VIIa (1:500, DSHB, MYO7A), rabbit anti-Sox2 (1:1000, Millipore, AB5603), rat anti-Sox2 (1:1000, Invitrogen, 14-9811-82), rabbit anti-GLUT1 (1:500, abcam, ab115730), mouse anti-ZO-1 (1:500, Invitrogen, 33-9100), mouse anti- E-Cadherin (1:200, BD Biosciences, 610181), and rabbit anti-connexin 31 (1:250, Proteintech Group, 12880-1-AP). The following secondary antibodies were used (1:500): Alexa Fluor 488 goat anti-chicken (Thermo Fisher Scientific, A11039), Alexa Fluor 488 goat anti-mouse (Thermo Fisher Scientific, A32723), Alexa Fluor 488 goat anti-rabbit (Thermo Fisher Scientific, A32731), Alexa Fluor 568 goat anti-mouse (Thermo Fisher Scientific, A-11004), Alexa Fluor 568 goat anti-rabbit (Thermo Fisher Scientific, A11036), Alexa Fluor 647 goat anti-mouse (Thermo Fisher Scientific, A32728), and Alexa Fluor 647 goat anti-rabbit (Thermo Fisher Scientific, A32733).

Confocal imaging and image analysis

To measure astrocyte morphology, fluorescent images were acquired using a Zeiss LSM 880 laser scanning confocal microscope with 63X oil immersion objective with frame size at 1024 x 1024 and bit depth at 12. Serial images at z axis were taken at an optical step of 1 mm, with overall z axis range encompassing the whole section. Images were imported to Imaris Bitplane software, and only astrocytes with their soma between

the z axis range were chosen for further analysis (Lanjakornsiripan et al., 2018). We performed 3D surface rendering using the Imaris Surface module, and color-coded the reconstructed surface images based on the surface area of each astrocyte. Morphological analysis was performed using the Imaris Filament module. Astrocyte branches and processes were outlined by Autopath with starting point set at 10 mm and seed point set at 0.5 mm, and statistical outputs including ‘‘filament number Sholl intersections’’ were extracted and plotted with Prism software. Data were generated from 3 brain sections per region per mouse with 3 mice per genotype. To analyze number of astrocytes and Med12 knockout efficiency, fluorescent images were acquired using a Zeiss LSM 880 laser scanning confocal microscope with 20X objective. Cell numbers were quantified by the QuPath software Cell Detection function (Bankhead et al., 2017). To examine the cochlea, fluorescent images were acquired using a Zeiss LSM 880 laser scanning confocal microscope with 20X objective.

Behavioral tests

Fear conditioning

Fear conditioning was performed as previously described (Samaco et al., 2008). Mice were tested at 4-month-old in a chamber that contains a grid floor that can deliver an electric shock (Actimetrics chamber system, Med Associates, St. Albans, VT, USA). On Day 1 of the test, mice were placed in the chamber and left undisturbed for 2 min followed by a 30 s white noise sound pulse (‘cue’). At the end of the cue, the mouse was shocked (2 s, 0.4 mA). 2 min later, a second pairing of sound cue followed by

206 shock was delivered. Thirty seconds after the final shock, the animal was removed and
207 replaced to the home cage. The following day, the animals were replaced to the same
208 chamber ('context test') and freezing behavior was recorded for 6 min. Freezing
209 behavior was recorded automatically by the instrument. One hour after the context test,
210 the animals were placed into a chamber which had been cleaned with an unfamiliar
211 agent (ethanol) and the wall color, the chamber shape and the odor (artificial vanilla)
212 had been changed to remove the contextual cues of the chamber. The animals were
213 then monitored for 3 min. After 3 min, the white noise cue was started and lasted 3 min.
214 The amount of freezing was recorded separately for the first 3 min and for the last 3 min
215 (cue test). The number of freezing intervals was converted to a percentage of freezing
216 for both the context test and the cue test, and the data were analyzed using a one-way
217 ANOVA.

218

219 *Acoustic startle response*

220 Acoustic startle response and prepulse inhibition was performed as previously
221 described (Samaco et al., 2008). Mice at 4-month old were subjected to acoustic
222 prepulse inhibition test. The acoustic prepulse inhibition task consists of presenting the
223 animal with two closely paired sound pulses: a prepulse at +0 dB, +4 dB (74 dB), +8 dB
224 (78 dB), +12 dB (82 dB) and over background followed 100 ms later by a pulse of 120
225 dB. The amount of startle the pulse induces in the animal is recorded using a startle
226 chamber for mice (SR-Lab, San Diego Instruments, San Diego, CA, USA) which
227 records activity for 65 ms after the pulse. The maximum amplitude recorded over the 65

ms is recorded and compared using an ANOVA. No prepulse inhibition result is presented because the Med12-deficient mice showed no acoustic startle response.

Auditory brainstem response recording

Auditory brainstem response recording was performed as previously described (Manalo et al., 2020). Mice were intraperitoneally injected with ketamine-xylazine (100: 10 mg/kg). Depth of anesthesia was verified by the absence of toe-pinch reflex. Testing was performed in a soundproof faraday cage booth while mice were placed on heating pad to maintain normal body temperature throughout the procedure. Pure tone bursts (0.1 ms rise/fall, 2 ms duration, 21 presentations/s) from 4 to 48 kHz were generated using System 3 digital signal processing hardware and software (Tucker Davis Technologies). The intensity of the tone stimuli was calibrated using a type 4938 one-quarter inch pressure-field calibration microphone (Bru¨el & Kjær). EC1 ultrasonic, low-distortion electrostatic speakers were coupled to the ear canal to deliver stimuli within 3 mm of the tympanic membrane. Response signals were recorded with subcutaneous needle electrodes inserted at the vertex of the scalp (channel 1), the postauricular bulla region (reference), and the back leg (ground), and averaged over 500 presentations of the tone bursts. Electrode-recorded activity was filtered (high pass, 300 Hz; low pass, 3 kHz; notch, 60 Hz) before averaging to minimize background noise. Auditory thresholds were determined by decreasing the sound intensity of each stimulus to 10 dB from 90 dB in 5 dB steps until the lowest sound intensity with reproducible and recognizable waveforms was detected. Thresholds were determined to within 5 dB for each frequency by two raters to ensure reliability. SD (dB SPL) were plotted as a function of

stimulus frequency (kilohertz) and analyzed for group differences by a two-way ANOVA, followed by a multiple-comparison test, to reveal overall trends.

Distortion Product Otoacoustic Emission

DPOAEs (2f1-f2) were measured from the left ears in sessions separate from ABR recording. Twelve A12-KO mice (3 female) and 9 A12-Con mice (1 female) were prepared as for ABR measures. Input/output curves were obtained for primary stimulus frequencies f1 and f2, where f1=f2/1.2 at fixed level differences L1 and L2, where L2=L1–10 dB. DPOAEs were measured for f2=12, 18, and 24 kHz, and L2 levels ranging from 0-80 dB SPL in 5 dB steps. Stimuli were presented using 2 TDT EC1 speakers configured in a closed acoustic system along with a Knowles probe microphone to record speaker and cochlear output. Primary and DPOAE levels were recorded using EMAV software in conjunction with TDT and custom hardware. DPOAE thresholds were defined as a 2f1-f2 response of at least -15 dB SPL. This level was chosen as it represented the lowest criterion response that was reliably above background noise levels and was generally within 10 dB of ABR thresholds.

Endocochlear Potential recording

EP recordings were obtained from the left ear of 10 A12-KO mice (2 female) and 9 A12-Con mice (1 female). To record the EP, animals were anesthetized with 80 mg/kg ketamine, 15 mg/kg xylazine, i.p., and positioned ventral-side-up in a custom head holder. Core temperature was maintained at 37.5 ± 1.0 ^{o}C using a DC electric

heating pad in conjunction with a rectal probe (FHC). After blunt dissection of the jaw musculature to reveal the left auditory bulla and opening of the posterior bulla with forceps, a hole was made in the cochlear capsule directly over scala media of the lower basal turn using a fine drill. Glass capillary pipettes (20-30 MΩ) filled with 0.15 M KCl were mounted on a hydraulic microdrive (Frederick Haer) and advanced until a stable positive potential was observed that did not change with increased electrode depth. The signal from the recording electrode was led to an AM Systems Model 1600 intracellular amplifier.

QUANTIFICATION AND STATISTICAL ANALYSIS

Sample sizes and statistical tests can be found in accompanying Figure legends. Offline analysis was carried out using SPSS 20 and Excel software. We assessed the significance of data for comparison by Student's two-tailed unpaired/paired t test or two-tailed unpaired t test. For multiple comparisons, we used the one-way ANOVA with Tukey's test and two-way ANOVA with Sidak's test. In general, we assumed data were normally distributed but this was not formally tested. Data are presented as mean ± SEM (standard error of the mean). Levels of statistical significance are indicated as follows: * ($p < 0.05$), ** ($p < 0.01$), *** ($p < 0.001$).

Results

Deletion of Med12 Selectively Reduces Morphological Complexity of Astrocytes

To decipher whether Med12 plays a role in astrocyte function in the adult brain, we evaluated its expression in astrocytes by co-immunostaining with GFP and Med12 in 16-week-old *Aldh1l1-GFP* reporter mice. This analysis revealed that approximately 70% of Aldh1l1-GFP astrocytes express Med12 in the olfactory bulb (73.1±2.3%) and around 50% across other examined brain regions (**Figures 1A-1D, 1R**, cortex: 52.0±2.3%, hippocampus: 48.5±8.8%, brainstem: 57.9±5.2%); Med12 also exhibited expression in NeuN positive neurons in these same brain regions.

Med12 plays an important role in numerous developing tissues, rendering the germline knockout embryonic lethal (Rocha et al 2010a, Rocha et al 2010b)and requiring the generation of temporal and lineage-specific knockout alleles to study its role in mature astrocytes. To specifically knock out *Med12* in astrocytes in the adult brain, we acquired mice containing a floxed Med12 allele (*Med12*$^{fl/fl}$) and intercrossed it with the *Aldh1l1-CreER* line and the *Aldh1l1-GFP* reporter, producing the *Aldh1l1-CreER; Aldh1l1-GFP; Med12*$^{fl/fl}$ and *Aldh1l1-CreER; Aldh1l1-GFP; Med12*$^{fl/y}$ (AG12) mouse line. Tamoxifen (TM) was administered at post-natal day 30 (P30), which allowed us to bypass possible developmental roles for Med12. Mice were harvested two months after TM treatment (P80-P90) and stained for Med12. We observed loss of Med12 in more than 50% of Aldh1l1-GFP positive astrocytes in the olfactory bulb, cortex, hippocampus, and brainstem two months after treatment **(Figures 1A–1H, 1R**; Aldh1l1-GFP astrocytes that express Med12 in AG12-Con: olfactory bulb: 73.1±2.3%, cortex: 52.0±5.1%, hippocampus: 48.5±8.8%, brainstem: 57.9±5.2%; in AG12-KO: olfactory bulb: 28.0±5.6%, cortex: 31.7±4.5%, hippocampus: 9.4±4.7%, brainstem:

28±12%). We were unable to achieve higher KO efficiency because prolonging TM treatment led to severe gastrointestinal illness, which ultimately resulted in death.

To determine whether deletion of Med12 impacts astrocyte homeostasis, we assessed their morphology using confocal imaging of the Aldh1l1-GFP reporter in AG12-Con and AG12-KO brains. Three-dimensional reconstructions of these images were subjected to Sholl Analysis to evaluate the morphological complexity of astrocytes. This analysis revealed that astrocytes from AG12-KO mice demonstrate reduced complexity in the prefrontal cortex and CA1 of the hippocampus, whereas astrocytes from the olfactory bulb and brainstem were unaffected (**Figures 1J-1Q; 1S-1V**). Quantification of the gross numbers of Sox9-expressing astrocytes did not reveal any differences between AG12-Con and AG12-KO mice (Aldh1l1-GFP^{+}/DAPI ratio in AG12-Con: olfactory bulb: 15.5±2.8%, cortex: 13.6±2.2%, hippocampus: 25.7±6.8%, brainstem: 10.3±2.3%; in AG12-KO: olfactory bulb: 14.9±1.6%, cortex: 15.6±1.9%, hippocampus: 26.1±2.7%, brainstem: 9.6±2.2%), indicating that loss of Med12 does not lead to cell death (**Figure 1W**). Together, these studies indicate that Med12 is selectively required to maintain the morphological complexity of astrocytes in the hippocampus and cortex, but is not required in the olfactory bulb or brainstem.

Elimination of Med12 Leads to Rapid Hearing Loss

The foregoing observation that loss of Med12 results in decreased morphological complexity of astrocytes in the hippocampus and prefrontal cortex, led us to examine whether these cellular phenotypes lead to behavioral deficits associated with these brain regions. Since the hippocampus demonstrated the most efficient knockout of

Med12, we conducted fear conditioning assays, which are associated with hippocampal function. As shown in Figure 2A, AG12-Con mice showed significantly increased freezing behaviors after the auditory cue (AG12-Con mice: no cue: 25.3±1.5%, cued: 75.2±3.2%); however, AG12-KO mice demonstrated no change in freezing before and during the auditory cue (**Figure 2A,** AG12-KO mice: no cue: 6.7±1.7%, cued: 17.1±5.4%). Further analysis revealed that the AG12-KO mice did not respond to acoustic stimulation (**Figure 2B,** AG12-Con mice: 2495.2±492.1 a.u., AG12-KO mice: 58.0±11.9 a.u.), indicating that the apparent deficits in fear conditioning are likely the result of impaired hearing. Consistent with this interpretation, we did not observe any changes in short term potentiation (STP) or long term potentiation (LTP) in the hippocampus of AG12-KO compared to AG12-Con (**Figure 2C-E,** LTP: AG12-Con mice: 120.69±14.43%, AG12-KO mice: 124.8±25.67%).

The loss of hearing in the AG12-KO mice prompted us to further examine auditory function by measuring auditory brainstem responses (ABRs). We first established a baseline ABR for AG12-Con and AG12-KO mice prior to TM-induced deletion of Med12, finding no differences in ABR thresholds between two groups **(Figure 3B,** 4 to 32 KHz). Next, we evaluated ABR in weekly intervals post-TM induced deletion (**Figure 3A**), finding dramatic elevation of auditory thresholds at one-week post-TM treatment (at 4 KHz, AG12-Con mice: 63.3±1.7dB SPL, AG12-KO mice: 77.9±4.9dB SPL. at 16 KHz, AG12-Con mice: 49.2±2.4dB SPL, AG12-KO mice: 65.7±6.3dB SPL), culminating in a complete loss of auditory response to all stimulation by three weeks post TM-treatment (**Figure 3C-3D,** 4 to 32 KHz, AG12-KO mice with no response). To identify the possible cause of hearing loss we further examined the

recording of auditory brainstem responses from each group at three weeks after TM induction. ABR responses at 8kHz in AG12-Con mice revealed five clearly defined maxima which represent major ABR peaks I to V (**Figure 3F**). In contrast, we did not observe any of the major ABR peaks in AG12-KO mice three weeks after TM (**Figure 3G**). ABR wave I corresponds to compound auditory nerve conduction, therefore its loss in the AG12-KO mice indicates that Med12 deletion results in dysfunction of the inner ear, which inhibits initiation of the auditory response.

Med12 is Required to Maintain the Structural Integrity of the Stria Vascularis

Having established that the loss of hearing in AG12-KO mice is likely due to defects in the inner ear, we next examined the cellular integrity of the cochlea. Starting with the organ of Corti, analysis of AG12-KO mice at three weeks post-TM induction did not reveal any overt structural changes in supporting cells (Sox2+) or hair cell (Myo7a+) populations (**Figure 4A-H**, 3 animals in each group were analyzed). Moreover, analysis at five weeks post-TM induction also did not show any changes in the cellular integrity of the organ of Corti (**Figure 4I-P**, 3 animals in each group were analyzed). However, analysis at 18 weeks post-TM induction did reveal an eventual loss of Myo7a-expressing hair cells, coupled with disorganization of Sox2-expressing support cells and a general breakdown in organ of Corti integrity (**Figure 4Q-X**, 3 animals in each group were analyzed). Nevertheless, the latent loss of hair cells at 18 weeks after Med12 deletion does not coincide with the observed loss of ABR at 2-3 weeks post-deletion (**Figure 3**), indicating that Med12-dependent loss of ABR is likely mediated through other cellular mechanisms in the adult cochlea.

Next, we examined additional structures in the cochlea, finding that Aldh1l1-GFP is also co-localized to the spiral ligament and basal cells of the stria vascularis (**Figure 5A-D).** Strikingly, at three weeks post-TM induction the stria vascularis of AG12-KO mice exhibited drastic alterations in its integrity, highlighted by alterations in the structure of ATP1A1-expressing intermediate cells at the apical turn (**Figure 5C-D v Figure 5G-H; yellow arrows**). Analysis at five weeks post-TM revealed that ATP1A1-expressing intermediate cells are completely lost from middle to apical turns in AG12-KO mice, which further disrupts the architecture of these structures (**Figure 5I-P**). Given the essential role of the stria vascularis in maintaining the ionic composition of endolymph, these findings suggest that progressive loss of the stria vascularis results in ionic imbalance of the endolymph, which compromises hair cell function, leading to hearing loss in AG12-KO mice.

To decipher which cell populations in the cochlea are dependent on Med12 expression, we used immunostaining to determine its pattern of expression. Staining for Med12 was observed in the stria vascularis in AG12-con mice three weeks post-TM induction (**Figure 5Q-R**). Nuclear localization of Med12 was observed in basal cells and fibrocytes in the spiral ligament (**Figure 5R, yellow arrowheads**). Analysis of Med12 expression in AG12-KO mice, revealed that the nuclear localized expression in basal cells was significantly decreased (**Figure 5R v 5T**). The percentage of Med12 positive basal cells reduced from 91.2±5.9% (AG12-con mice, n=3) to 25.1±1.2% (AG12-KO mice, n=3) (**Figure 5W**). These observations suggest that Med12 deletion is occurring in the basal cells of the stria vascularis in the AG12-KO mouse line.

Med12 Deletion Disrupts Basal Cell Organization

To track which populations in the cochlea undergo TM-induced Cre-recombination in the Aldh1l1-CreER line we replaced the Aldh1l1-GFP reporter with a Cre-inducible reporter, generating the *Aldh1l1-CreER; Rosa-CAG-LSL-tdTomato; Med12$^{fl/f}$* mouse line (i.e. AT12 line). We treated AT12-Con mice with TM and harvested the cochlea two weeks after induction, finding that the tdTomato reporter labeled the Glut1-expressing basal cells of the stria vascularis and some fibrocytes in the spiral ligament (**Figure 6A-D; yellow arrowheads**), but not spiral ganglion cells (not shown)**.** Consistent with a requirement for Med12 expression in basal cells, examination of AT12-KO mice two weeks after TM induction revealed a loss of basal cell organization, where Glut1- and tdTomato- expressing basal cells appear diffuse and lose cell-cell contact (**Figure 6E-H; unfilled arrowheads,** 3 animals in each group analyzed, phenotype observed in all AT12-KO mice). Together, these finding indicate that Med12 is required to maintain the organization and integrity of basal cells in the stria vacularis.

Adhesion between cell types within the stria vascularis is required to generate and preserve ion gradients in the endolymph, which are essential for maintaining endocochlear potential and auditory function (Ciuman 2009, Wan et al 2013). Our observed cellular phenotypes in basal cells of the AT12-KO line suggests that cell adhesion within the stria vascularis is disrupted. To test this, we evaluated the expression of key junction proteins associated with hearing loss in this region, ZO1, E-cadherin (Ecad), and Connexin 31 (Cx31). In AT12-Con animals, ZO1 is concentrated next to the cell membrane of basal cells, however, ZO1 expression level was dramatically decreased in AT12-KO mice (**Figure 6I-L; white arrowheads**, the intensity

ratio reduced to 0.696±0.026 compared to AT12-Con, n=3 in each group). Cx31 protein was highly concentrated between basal cells and fibrocytes in spiral ligament in AT12-Con mice and demonstrated disorganized localization in AT12-KO mice (**Figure 6M-P, white arrowheads; Figure 6U** the intensity ratio was reduced to 0.689±0.103 compared to AT12-Con, n=3 in each group**)**. Ecad expression was mainly observed in both intermediate cells and basal cells (**Figure 6Q-R**). Although the distribution of Ecad was altered in AT12-KO mice (**Figure 6S-T**), the intensity was not significantly different compared to AT12-Con mice (**Figure 6Q-T, U,** intensity ratio: 1.036±0.047 compared to AT12-Con, n=3 in each group). These finding suggested that Med12 is necessary to maintain the expression of these critical junction and cell adhesion proteins in the stria vascularis and spiral ligament.

Reduced Endocochlear Potential in Med12 Mutant Mice

The forging studies indicate that loss of Med12 disrupts the organization of the basal cells as early as two weeks after TM-induced deletion, suggesting that the cascade of cellular events that lead to hearing loss originates in the stria vascularis. Therefore, we next measured the endocochlear potential (EP) in AG12-Con and AG12-KO mice 10-14 days after TM-induced deletion. Consistent with our prior results (**Figure 3**), AG12-KO mice showed ABR thresholds that were 15-25 dB higher than those in AA2-Con mice. These differences were significant overall ($p<.001$), with no interactions by frequency (**Figure 7A**). The overall relative 'flat' threshold shift in the AG12-KO mice compared to AG12-Con supports a non-frequency specific influence, consistent with isolated strial dysfunction (Schuknecht and Gacek,1993). EP recordings from the same cochleas

(**Figure 7B**) revealed no overlap of EP values by group ($p<.001$), with AG12-Con showing typical values for C57BL/6 mice (>100 mV) (Ohlemiller, et al. 2009) and AG12-KO mice averaging ~30 mV lower (76.8 versus 106.7 mV).

To confirm that these mice, at this timepoint, have stria-specific defects we next performed distortion product otoacoustic emission (DPOAE) tests on these same mice (Ueberfuhr, et al 2016). In the presence of an isolated strial defect, maximum DPOAE values should be similar for normal and stria-impaired mice, and DPOAE thresholds should be spared relative to ABR thresholds at the same frequencies (Mills, 2003). Since the DPOAE input/output results did not vary with f2 frequency, data from f2 = 12, 12, 24 kHz were all included from each animal. This analysis revealed that the maximum DPOAE values did not differ significantly between AG12-Con and AG12-KO mice, although control mice gave slightly higher values (30.5 versus 36.2 dB SPL) (**Figure 7C**). Finally, a stria-specific defect is also predicted to yield DPOAE thresholds that are lower relative to ABR thresholds, meaning that ABR-DPOAE threshold differences should be higher when stria is compromised. Indeed, this metric both averaged (0.83 versus -5.04) and skewed higher in the AG12- KO (**Figure 7D**), supporting the existence of isolated strial dysfunction in the majority of the AG12-KO mice. In sum, ABR, EP, and DPOAE data supported a central tendency toward isolated strial dysfunction in the AG12-KO mice as early as 10-14 days after TM induced deletion.

Discussion

Mutations in MED12 are linked to a broad spectrum of genetic disorders with X-linked intellectual disability (Donnio et al 2017, Lesca et al 2013, Rubinato et al 2020, Schwartz et al 2007, Vulto-van Silfhout et al 2013), however embryonic lethality in Med12-null and heterozygous mice have hindered the study of these Med12-associated phenotypes (Rocha et al 2010a, Rocha et al 2010b) Here, we applied temporal and tissue-specific approaches to study Med12 function in adult astrocytes in the CNS. Critically, the lethality rate dramatically increased with prolonged Tamoxifen treatment, which likely prevented us achieving a high KO efficiency in astrocytes in the CNS (see figure 1R). This technical limitation may have masked some CNS related phenotypes associated with Med12 function. Surprisingly, we found that Aldh1l1-CreER mediated Med12 deletion in the adult led to rapid hearing loss. Although hearing loss has been reported in cases of Med12-related disorders (Rubinato et al 2020) the underlying mechanisms remained undefined. We found that Med12 is necessary for maintaining the integrity of the stria vascularis in the adult, likely by regulating the expression of ZO-1, E-cadherin, and Cx31. These changes in gene expression alter cell adhesion between basal cells and the spiral ligament, which would likely impede the generation of normal endolymph and culminates in loss of hair cell mechanotransduction.

Our studies revealed that basal cells and the spiral ligament of the adult cochlea are transcriptionally dependent on Med12 to maintain their overall structural integrity. We recently identified similar transcriptional dependencies in the adult brain, where the transcription factor NFIA is required to maintain the morphological complexity of hippocampal astrocytes (Huang et al 2020). Together, these studies highlight adult- and region- specific roles for developmental transcription factors in maintaining key aspects

of cell structure in mature populations. Med12 functions, in part, to maintain the expression of key proteins that maintain tight junctions (TJs) and gap junctions (GJs), which are critical for normal cochlear function (Wan et al 2013, Wangemann 2006). Prior studies indicate that genetic deletion of either E-cadherin (Trowe et al 2011), or Cx31 (Lopez-Bigas et al 2001) during development results in hearing loss, suggesting that their regulation by Med12 contributes to the observed hearing loss in the adult. While our studies suggest that downregulation of these structural proteins is responsible for the effects of Med12-loss in the cochlea, it is possible that Med12 regulates the expression of other genes that are also important for these effects. Further studies on Med12 target gene networks in basal cells will be critical for deciphering these regulatory networks and associated mechanisms.

Our findings demonstrate that loss of Med12 in basal cells and the spiral ligament leads to defects of the stria vascularis. Progressive degeneration of the stria vascularis underlies a form of age-related hearing loss known as strial or metabolic presbycusis (Schuknecht & Gacek 1993). However, we cannot exclude the possibility that loss of Med12 in other tissues contributes to hearing loss in humans. Med12 expression is also observed in supporting cells in cochlea and in major cell types in nervous system, raising the possibility that it has related functions in these systems. Nevertheless, our study describes the first animal model that recapitulates hearing loss identified in Med12-related disorders and provides a new system in which to examine the underlying cellular and molecular mechanisms. Moreover, the TJ and GJ proteins that are downregulated in the Med12-deficient cochlea also play important roles in other systems; for example, ZO1 is highly expressed in circumventricular organs of the CNS

and is required for the integrity of blood brain barrier (Petrov et al 1994), and a Cx31 mutation leads to peripheral neuropathy in addition to sensorineural hearing impairment in patients (Lopez-Bigas et al 2001). Therefore, our studies lay the foundation for further examination of Med12 function in other systems linked to Med12-disorders.

To ascertain whether the initial defects in the AG12-KO cochlea are due to strial dysfunction we measured a series of physiological parameters associated with cochlear function at timepoints where basal cell organization is altered and the organ of corti is intact. The most essential evidence for strial pathology in the AG12-KO mouse derives from direct EP recordings, where AG12-KO and AG12-Con mice showed no overlap of EP values, with the AG12-KO averaging ~30 mV decrease in EP. Thus, all of the AG12-KO mice exhibited the single functional requirement for strial pathology, although this does not directly address whether other defects are present at these relatively early timepoints (i.e. 10-14 days post-TM). Other evidence for strial-specific defects at these early timepoints are based on no changes in the DPOAE input/output data between the AG12-KO and AG12-Con, coupled with a relative sparing of DPOAE thresholds versus ABR (DPOAE-ABR) thresholds at the same frequency (Mills, et al. 2003) which yielded higher positive values (ABR threshold higher) in the AG12-KO line. In sum, four functional metrics supported an initial, delimited, strial pathology in AA12-KO mice. EP reduction was the requisite criterion, but since EP recording is a terminal procedure it cannot be used clinically. While we did not first conceive of the threshold and DPOAE-based metrics we used to evaluate strial pathology in our AG12-KO mice, we believe we are the first to apply all three criteria. The principal limitation to such an approach at present is simply the lack of suitable models. Thus, the Med12 KO model may

548 represent a useful system for additional studies aimed at detecting and characterizing
549 isolated chronic EP reduction.

550

551 **References**

552 Allen NJ, Lyons DA. 2018. Glia as architects of central nervous system formation and
553 function. *Science* 362: 181-85
554 Boettger T, Hubner CA, Maier H, Rust MB, Beck FX, Jentsch TJ. 2002. Deafness and
555 renal tubular acidosis in mice lacking the K-Cl co-transporter Kcc4. *Nature* 416:
556 874-8
557 Brownell WE, Bader CR, Bertrand D, de Ribaupierre Y. 1985. Evoked mechanical
558 responses of isolated cochlear outer hair cells. *Science* 227: 194-6
559 Chan DK, Hudspeth AJ. 2005. Mechanical responses of the organ of corti to acoustic
560 and electrical stimulation in vitro. *Biophys J* 89: 4382-95
561 Chen J, Zhao HB. 2014. The role of an inwardly rectifying K(+) channel (Kir4.1) in the
562 inner ear and hearing loss. *Neuroscience* 265: 137-46
563 Ciuman RR. 2009. Stria vascularis and vestibular dark cells: characterisation of main
564 structures responsible for inner-ear homeostasis, and their pathophysiological
565 relations. *J Laryngol Otol* 123: 151-62
566 Donnio LM, Bidon B, Hashimoto S, May M, Epanchintsev A, et al. 2017. MED12-related
567 XLID disorders are dose-dependent of immediate early genes (IEGs) expression.
568 *Hum Mol Genet* 26: 2062-75
569 Freeman MR, Rowitch DH. 2013. Evolving concepts of gliogenesis: a look way back
570 and ahead to the next 25 years. *Neuron* 80: 613-23
571 Grunder S, Muller A, Ruppersberg JP. 2001. Developmental and cellular expression
572 pattern of epithelial sodium channel alpha, beta and gamma subunits in the inner
573 ear of the rat. *Eur J Neurosci* 13: 641-8
574 Gulley RL, Reese TS. 1976. Intercellular junctions in the reticular lamina of the organ of
575 Corti. *J Neurocytol* 5: 479-507
576 Huang AY, Woo J, Sardar D, Lozzi B, Bosquez Huerta NA, et al. 2020. Region-Specific
577 Transcriptional Control of Astrocyte Function Oversees Local Circuit Activities.
578 *Neuron* 106: 992-1008 e9
579 John Lin CC, Yu K, Hatcher A, Huang TW, Lee HK, et al. 2017. Identification of diverse
580 astrocyte populations and their malignant analogs. *Nat Neurosci* 20: 396-405
581
582 Khakh BS, Deneen B. 2019. The Emerging Nature of Astrocyte Diversity. *Annu Rev*
583 *Neurosci* 42: 187-207
584 Lesca G, Moizard MP, Bussy G, Boggio D, Hu H, et al. 2013. Clinical and
585 neurocognitive characterization of a family with a novel MED12 gene frameshift
586 mutation. *Am J Med Genet A* 161A: 3063-71

587 Lopez-Bigas N, Olive M, Rabionet R, Ben-David O, Martinez-Matos JA, et al. 2001.
588 Connexin 31 (GJB3) is expressed in the peripheral and auditory nerves and
589 causes neuropathy and hearing impairment. *Hum Mol Genet* 10: 947-52
590 Loponen H, Ylikoski J, Albrecht JH, Pirvola U. 2011. Restrictions in cell cycle
591 progression of adult vestibular supporting cells in response to ectopic cyclin D1
592 expression. *PLoS One* 6: e27360
593 Mittal R, Aranke M, Debs LH, Nguyen D, Patel AP, et al. 2017. Indispensable Role of
594 Ion Channels and Transporters in the Auditory System. *J Cell Physiol* 232: 743-
595 58
596 Mills, D.M., 2003. Differential responses to acoustic damage and furosemide in auditory
597 brainstem and otoacoustic emission measures. . The Journal of the Acoustical Society
598 of America 113**,** 914-924.

599 Muller U. 2008. Cadherins and mechanotransduction by hair cells. *Curr Opin Cell Biol*
600 20: 557-66
601 Nagai J, Yu X, Papouin T, Cheong E, Freeman MR, et al. 2020. Behaviorally
602 consequential astrocytic regulation of neural circuits. *Neuron*
603 Nin F, Yoshida T, Sawamura S, Ogata G, Ota T, et al. 2016. The unique electrical
604 properties in an extracellular fluid of the mammalian cochlea; their functional
605 roles, homeostatic processes, and pathological significance. *Pflugers Arch* 468:
606 1637-49
607 Oesterle EC, Campbell S, Taylor RR, Forge A, Hume CR. 2008. Sox2 and JAGGED1
608 expression in normal and drug-damaged adult mouse inner ear. *J Assoc Res*
609 *Otolaryngol* 9: 65-89
610 Ohlemiller, K.K., 2009. Mechanisms and genes in human strial presbycusis from animal
611 models. Brain Research. 1277, 70-83.

612 Patuzzi R. 2011. Ion flow in stria vascularis and the production and regulation of
613 cochlear endolymph and the endolymphatic potential. *Hear Res* 277: 4-19
614 Petrov T, Howarth AG, Krukoff TL, Stevenson BR. 1994. Distribution of the tight
615 junction-associated protein ZO-1 in circumventricular organs of the CNS. *Brain*
616 *Res Mol Brain Res* 21: 235-46
617 Rocha PP, Bleiss W, Schrewe H. 2010a. Mosaic expression of Med12 in female mice
618 leads to exencephaly, spina bifida, and craniorachischisis. *Birth Defects Res A*
619 *Clin Mol Teratol* 88: 626-32
620 Rocha PP, Scholze M, Bleiss W, Schrewe H. 2010b. Med12 is essential for early mouse
621 development and for canonical Wnt and Wnt/PCP signaling. *Development* 137:
622 2723-31
623 Rozengurt N, Lopez I, Chiu CS, Kofuji P, Lester HA, Neusch C. 2003. Time course of
624 inner ear degeneration and deafness in mice lacking the Kir4.1 potassium
625 channel subunit. *Hear Res* 177: 71-80
626 Rubinato E, Rondeau S, Giuliano F, Kossorotoff M, Parodi M, et al. 2020. MED12
627 missense mutation in a three-generation family. Clinical characterization of
628 MED12-related disorders and literature review. *Eur J Med Genet* 63: 103768
629 Schuknecht HF, Gacek MR. 1993. Cochlear pathology in presbycusis. *Ann Otol Rhinol*
630 *Laryngol* 102: 1-16

631 Schwartz CE, Tarpey PS, Lubs HA, Verloes A, May MM, et al. 2007. The original Lujan
632 syndrome family has a novel missense mutation (p.N1007S) in the MED12 gene.
633 *J Med Genet* 44: 472-7
634 Stolt CC, Rehberg S, Ader M, Lommes P, Riethmacher D, et al. 2002. Terminal
635 differentiation of myelin-forming oligodendrocytes depends on the transcription
636 factor Sox10. *Genes Dev* 16: 165-70
637 Trowe MO, Maier H, Petry M, Schweizer M, Schuster-Gossler K, Kispert A. 2011.
638 Impaired stria vascularis integrity upon loss of E-cadherin in basal cells. *Dev Biol*
639 359: 95-107
640 Ueberfuhr, M.A., Fehlberg, H., Goodman, S.S., Withnell, R.H., 2016. A DPOAE
641 assessment of outer hair cell integrity in ears with age-related hearing loss. Hearing
642 Research. 332**,** 137-150.
643 Vogl MR, Reiprich S, Kuspert M, Kosian T, Schrewe H, et al. 2013. Sox10 cooperates
644 with the mediator subunit 12 during terminal differentiation of myelinating glia. *J*
645 *Neurosci* 33: 6679-90
646 Vulto-van Silfhout AT, de Vries BB, van Bon BW, Hoischen A, Ruiterkamp-Versteeg M,
647 et al. 2013. Mutations in MED12 cause X-linked Ohdo syndrome. *Am J Hum*
648 *Genet* 92: 401-6
649 Wan G, Corfas G, Stone JS. 2013. Inner ear supporting cells: rethinking the silent
650 majority. *Semin Cell Dev Biol* 24: 448-59
651 Wangemann P. 2006. Supporting sensory transduction: cochlear fluid homeostasis and
652 the endocochlear potential. *J Physiol* 576: 11-21
653 Watanabe K, Takeda K, Katori Y, Ikeda K, Oshima T, et al. 2000. Expression of the
654 Sox10 gene during mouse inner ear development. *Brain Res Mol Brain Res* 84:
655 141-5

656

657 **Figure Legends**

658

659 **Figure 1: Deletion of Med12 in Mature Astrocytes Selectively Reduces**

660 **Morphological Complexity**

661 **(A–H)** Co-expression of Med12 and Aldh1l1-GFP in AG12-Con and AG12-KO mice.

662 Filled arrowheads show co-expression of Aldh1l1-GFP and Med12; unfilled show

663 Aldh1l1-GFP cells that do not express Med12. **(I)** Tamoxifen treatment paradigm. **(J–Q)**

664 High-magnification confocal images of Aldh1l1-GFP from AG12-Con or AG12-KO mice

665 showing reduced complexity in the cortex and hippocampus. **(R)** Quantification of

Med12/Aldh1l1-GFP co-expression in AG12-Con and AG12-KO mice. Data are derived from 3 mice per genotype, 3 slides per region, per mouse: at least 500 cells per region, per mouse. One-way ANOVA. **(S–V)** Scholl analysis of astrocyte complexity in the cortex, olfactory bulb, brainstem, and hippocampus. Data are derived from 3 mice per genotype, 3 slides per region, per mouse, with at least 30 cells per region, per genotype; Two-way repeated-measures ANOVA. **(W)** Quantification of Aldh1l1-GFP/DAPI co-expression in AG12-Con and AG12-KO mice. Data are derived from 3 mice per genotype, 3 slides per region, per mouse: at least 500 cells per region, per mouse. One-way ANOVA.

Figure 2. Deletion of Med12 Results in Hearing Loss and No Changes in Synaptic Plasticity in the Hippocampus

(A) Quantification of freezing in cued fear conditioning and **(B)** startle responses in acoustic startle. In A, 4 AG12-Con and 5 AG12-KO mice were used; in B, 3 AG12-Con and 4 AG12-KO mice were used. Two-tailed unpaired t test. AG12-Con denotes Med12fl/fl; Aldh1l1-GFP and Med12fl/y; Aldh1l1-GFP. AG12-KO denotes Med12fl/fl; Aldh1l1-CreER; Aldh1l1-GFP and Med12fl/y; Aldh1l1-CreER; Aldh1l1-GFP. *$p < 0.05$; **$p < 0.01$. **(C)** Schematic of LTP recording experimental setting. **(D)** LTP traces from AG12-Con and AG12-KO hippocampal slices. **(E)** Quantification of LTP. All electrophysiological experiments are derived from 3 mice from each genotype, ranging from 7 to 13 cells total for each experiment. LTP: long-term potentiation; STP: short term potentiation; NS: no significance; *$p < 0.05$; **$p < 0.001$; Student's two-tailed paired **(L)** t test. AG12-Con denotes Med12fl/fl; Aldh1l1-GFP and Med12fl/y; Aldh1l1-

GFP. AG12-KO denotes Med12fl/fl; Aldh1l1-CreER; Aldh1l1-GFP and Med12fl/y; Aldh1l1-CreER; Aldh1l1-GFP.

Figure 3. Med12 Deletion Causes Rapid Peripheral Hearing Loss in Adult Mice

(A) Tamoxifen treatment paradigm for weekly auditory brainstem response (ABR) tests. **(B-E)** ABR thresholds at different frequencies before **(B)**, post-1-week **(C)**, post-2-weeks **(D)**, and post-3-weeks **(E)** of the tamoxifen treatment. Dashed lines mark the maximum pressure, 90dB, used in the tests. In **(B)**, 9 AG12-Con and 8 AG12-KO mice were recorded; in **(C)**, 6 AG12-Con and 7 AG12-KO mice were recorded; in **(D)**, 4 AG12-Con and 6 AG12-KO mice were recorded; in **(E)**, 9 AG12-Con and 10 AG12-KO mice were recorded. **(F-G)** ABR to stimuli of 60-90 dB sound pressure level (8 kHz) in AG12-Con **(F)** and AG12-KO **(G)** mice. AG12-Con denotes Med12fl/fl; Aldh1l1-GFP and Med12fl/y; Aldh1l1-GFP. AG12-KO denotes Med12fl/fl; Aldh1l1-CreER; Aldh1l1-GFP and Med12fl/y; Aldh1l1-CreER; Aldh1l1-GFP. Two-way repeated-measures ANOVA. *p < 0.05; **p < 0.01.

Figure 4: Deletion of Med12 has Latent Effects on the Structure of Organ of Corti

(A-X) Detection of the markers of supporting cells, Sox2, and hair cells, Myo7a, by immunofluorescence on midmodiolar sections of cochleae of AG12-Con and AG12-KO mice. Figures show the organ of corti in the basal turn. **(A-H)** A Comparison of midmodiolar sections of cochleae of AG12-Con and AG12-KO mice 3 weeks post-TM, **(I-P)** 5 weeks post-TM. **(Q-X)** 18 weeks post-TM. AG12-Con denotes Med12fl/fl;

Aldh1l1-GFP and Med12fl/y; Aldh1l1-GFP. AG12-KO denotes Med12fl/fl; Aldh1l1-CreER; Aldh1l1-GFP and Med12fl/y; Aldh1l1-CreER; Aldh1l1-GFP. TM: Tamoxifen treatment. Scale bar in D is 20 μm.

Figure 5: Med12 Expression in Basal Cells is Required to Maintain the Stria Vascularis

(A-P) Detection of the stria vascularis marker, ATP1A1, by immunofluorescence on midmodiolar sections of cochleae of AG12-Con and AG12-KO mice. Figures show the stria vascularis in the apical turn. Yellow arrowheads mark the regions of stria vascularis. **(A-H)** A Comparison of midmodiolar sections of cochleae of AG12-Con and AG12-KO mice 3 weeks post-TM, **(I-P)** 5 weeks post-TM. **(Q-T)** Immunostaining of Med12 in stria vascularis of midmodiolar sections of cochleae of AG12-Con and AG12-KO mice at 2 weeks post-TM. Figures show the stria vascularis in the middle turn. **(R)** and **(T)** are the regions from dashed squares in **(Q)** and **(S)**. Unfilled arrowheads mark the side of intermediate cells; yellow arrowheads mark the side of basal cells and the spiral ligament. AG12-Con denotes Med12fl/fl; Aldh1l1-GFP and Med12fl/y; Aldh1l1-GFP. AG12-KO denotes Med12fl/fl; Aldh1l1-CreER; Aldh1l1-GFP and Med12fl/y; Aldh1l1-CreER; Aldh1l1-GFP. TM: Tamoxifen treatment. **U** Quantification of Med12 expression in Aldh1l1-GFP basal cells; *$p<0.05$. Scale bar in **D** is 50 μm and **Q** is 20 μm.

Figure 6: Med12 is Required to Maintain Expression of Cell Adhesion Proteins

(A-H) Detection of Glut1, endothelial and basal cell marker, by immunofluorescence on midmodiolar sections of cochleae of AT12-Con and AT12-KO mice at 2 weeks post-TM. Figures show the stria vascularis in the middle turn. **(B-C)** Yellow arrowheads denote Glut1-positive basal cells, labeled by AT12-Con tdTomato reporter; **(F-G)** Unfilled arrowheads denote disorganized Glut-1/tdTomato basal cells in AT12-KO. **(I-T)** Detection of ZO1, E-cadherin, and Connexin-31 proteins by immunofluorescence on midmodiolar sections of cochleae of AG12-Con and AG12-KO mice at 2 weeks post-TM. **(I,M,Q)** Filled arrowheads denote AG12-Con expression of makers. **(K,O,S)** Unfilled arrows denote altered expression of markers in AG12-KO. **U** Quantification of immunostaining from I-T; *p<0.05. Scale bars in **D** and **L** are 50 μm.

Figure 7: Loss of Med12 Results in Stria Vascularis-Specific Defects

(A) ABR thresholds were significantly higher in KOs versus controls (2-way ANOVA, $F=46.188$, $DF=6$, $p<0.001$) with no significant interactions. **(B)** EPs were significantly lower in KOs (t-test for unequal variance, $DF=11$, $t=-7.23$, $p<0.001$). **(C)** 2f1-f2 maximum values were not significantly different by group (t-test for unequal variance, $DF=60$, $t=-1.84$, $p<0.07$). **(D)** Difference in ABR versus DPOAE threshold (ABR-DPOAE for -15 dB SPL criterion) was significantly higher in KOs (t-test for unequal variance, $DF=59$, $t=2.32$, $p<0.02$). DPOAE metrics were derived from input/output curves for f2=12, 18, and 24 kHz (See horizontal bar in A). Since these curves did not differ by f2 (not shown), data from all three frequencies were included in C and D

Figure 1

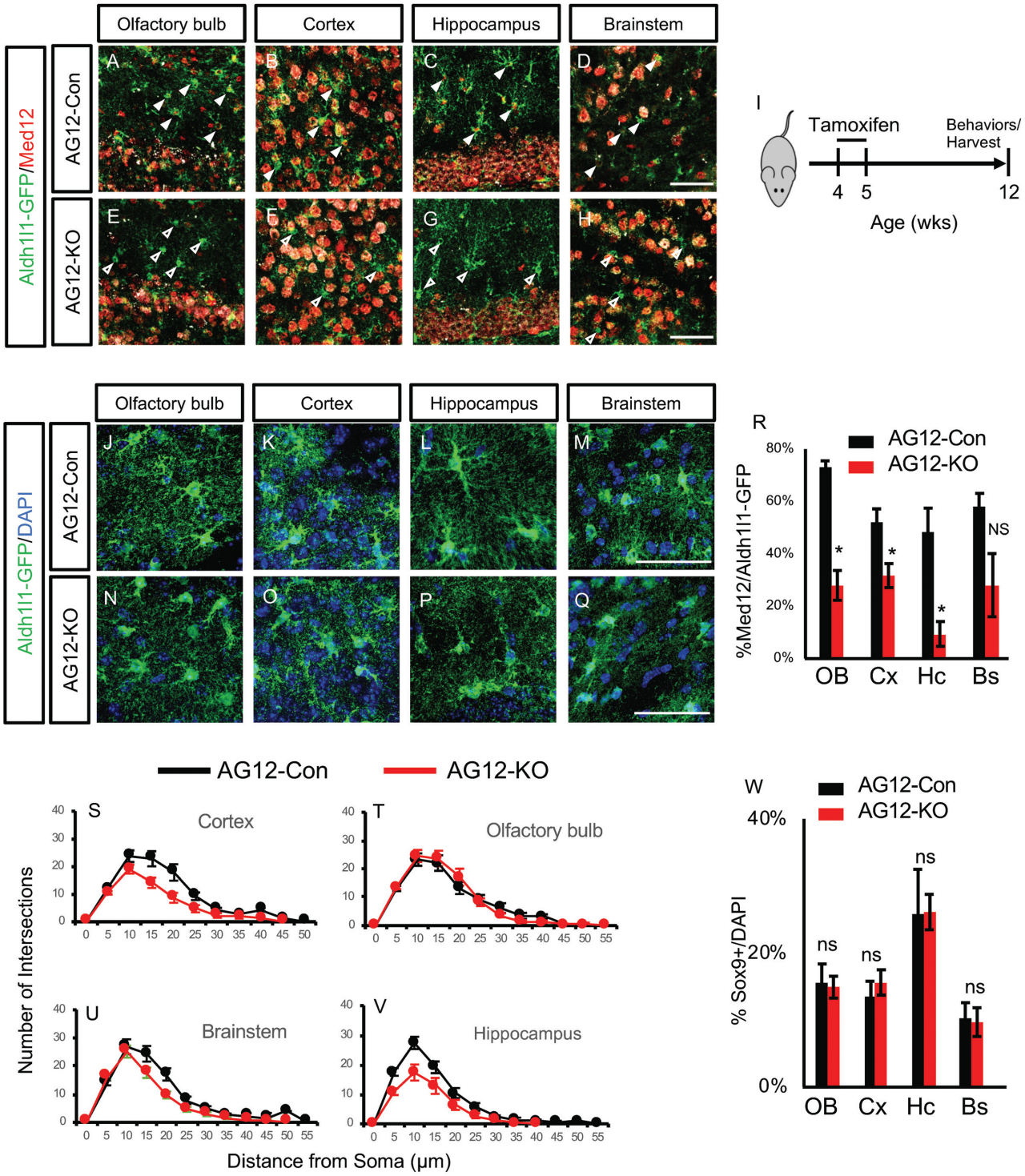

Figure 2

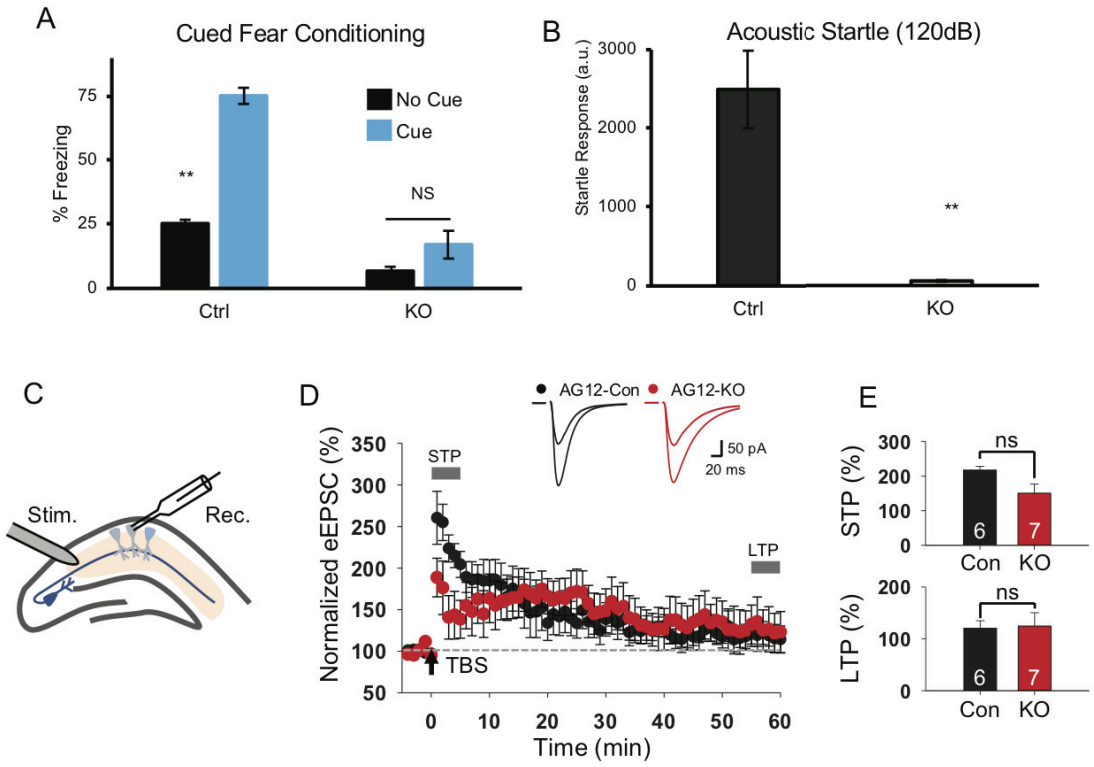

Figure 3

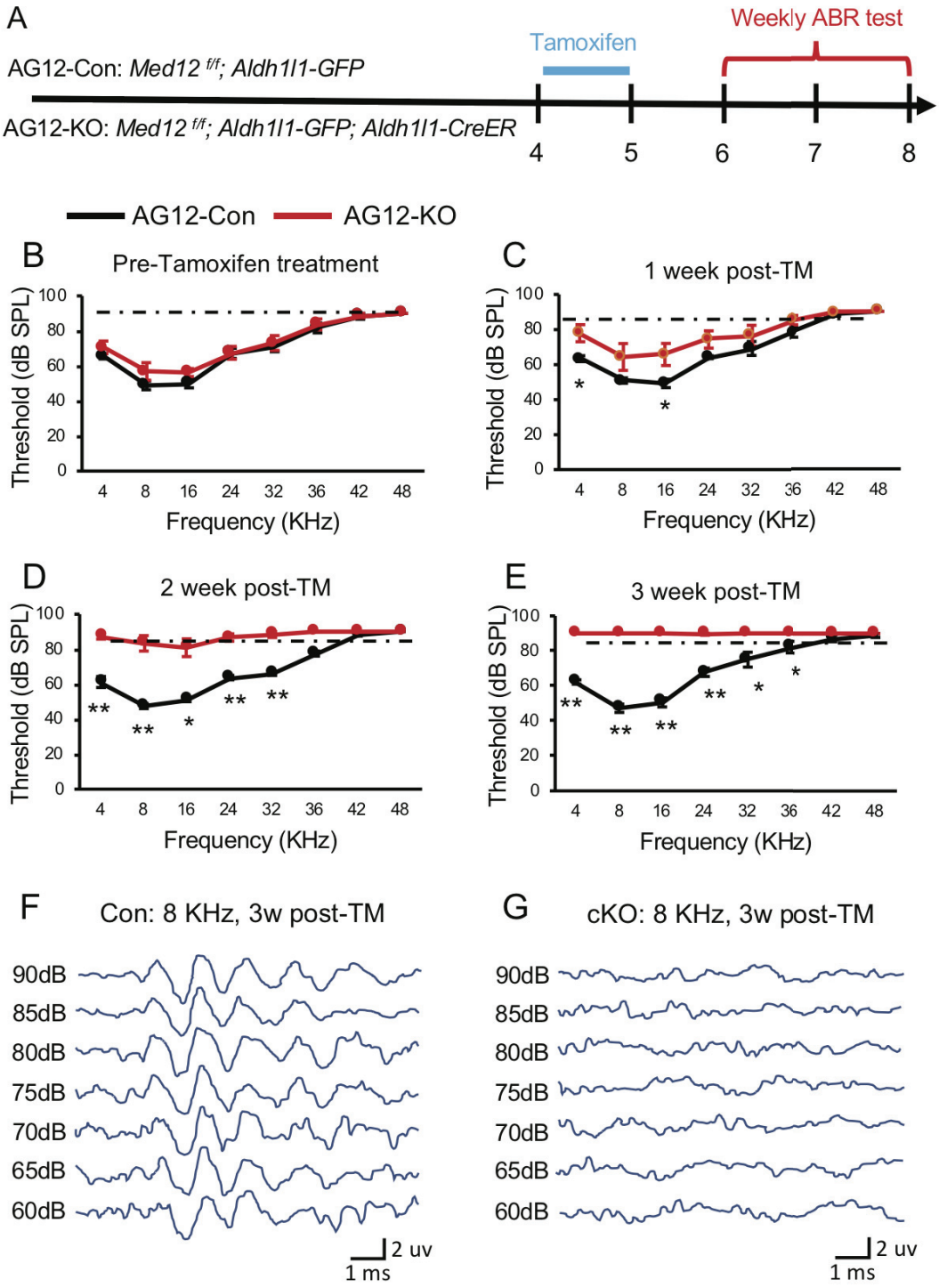

Figure 4

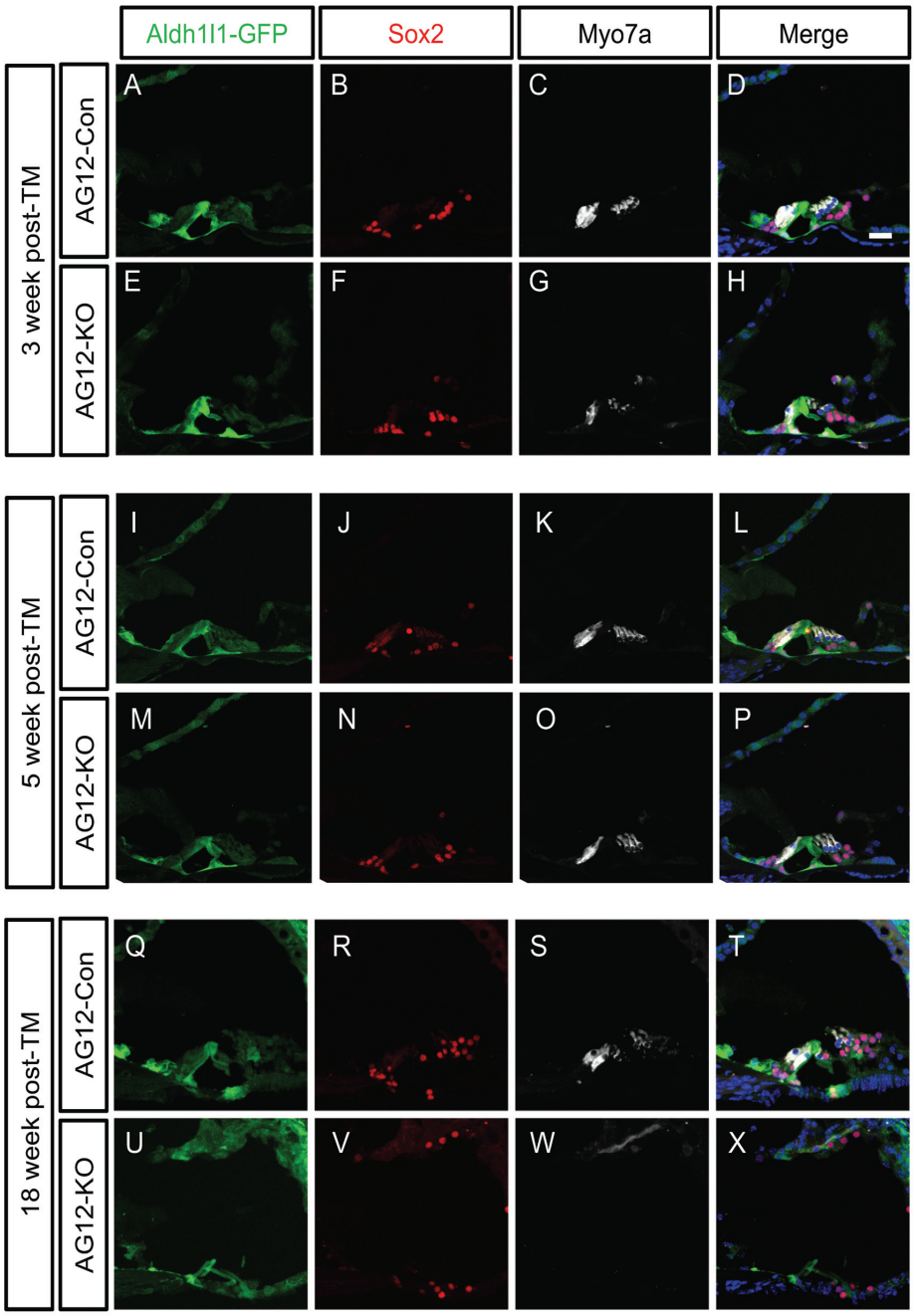

Figure 5

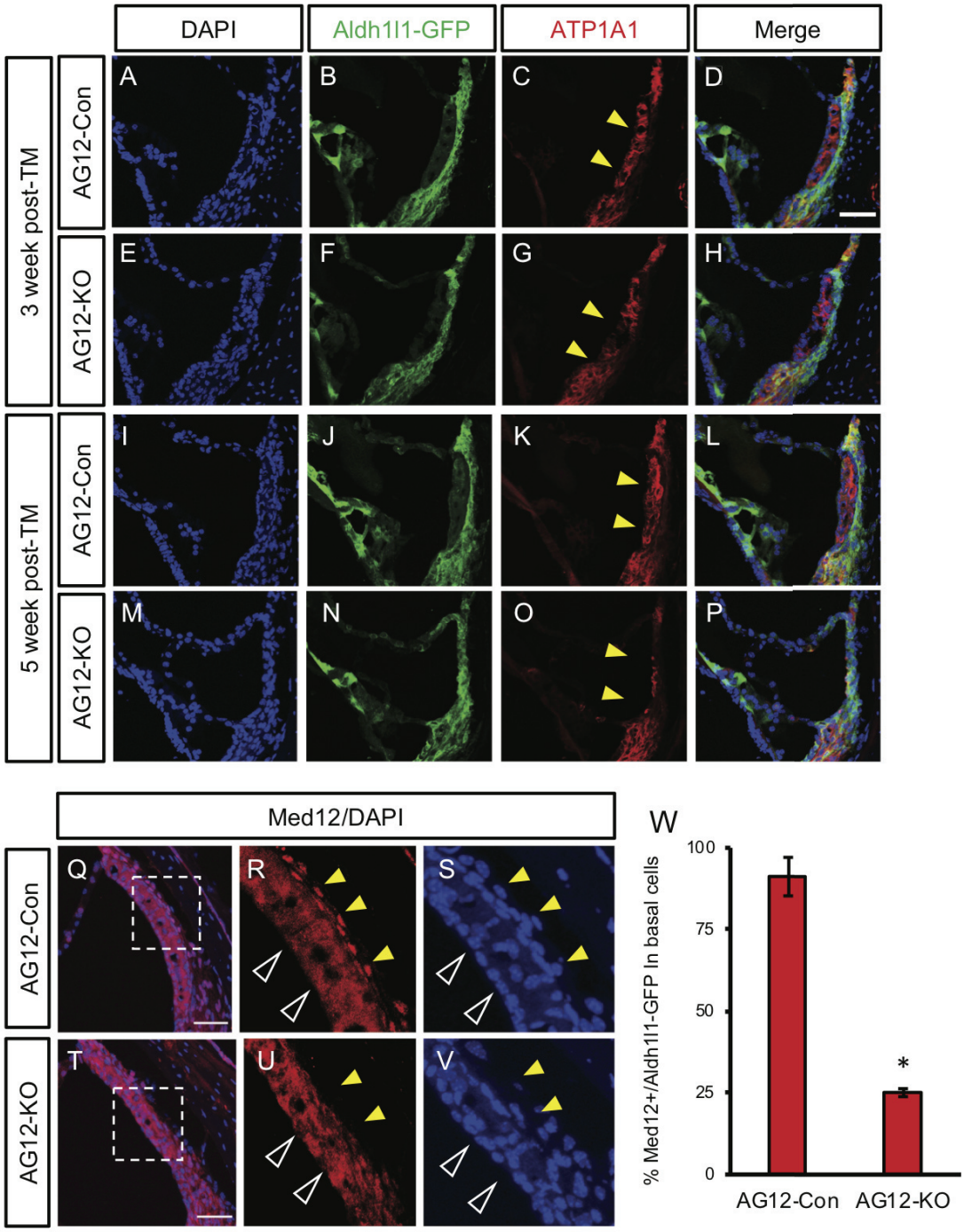

Figure 6

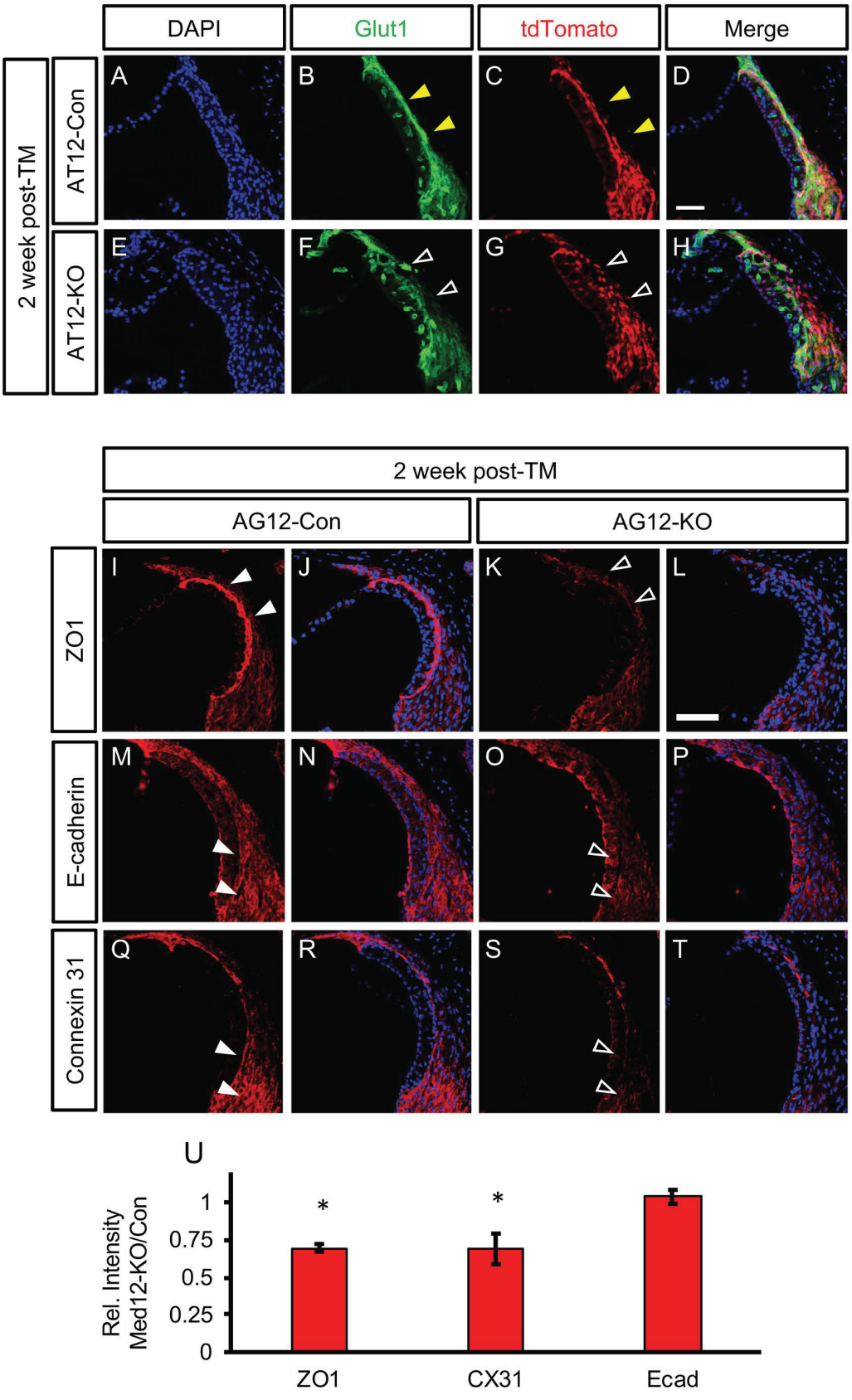

Figure 7